HHS Public Access

Author manuscript

Genet Med. Author manuscript; available in PMC 2022 March 25.

Published in final edited form as:

Genet Med. 2021 October ; 23(10): 1933–1943. doi:10.1038/s41436-021-01239-1.

Biallelic variants in *KARS1* are associated with neurodevelopmental disorders and hearing loss recapitulated by the knockout zebrafish

A full list of authors and affiliations appears at the end of the article.

Abstract

Purpose: Pathogenic variants in Lysyl-tRNA synthetase 1 (KARS1) have increasingly been recognized as a cause of early-onset complex neurological phenotypes. To advance the timely diagnosis of KARS1-related disorders, we sought to delineate its phenotype and generate a disease model to understand its function in vivo.

Method: Through International collaboration, we identified 22 affected individuals from 16 unrelated families harboring biallelic KARS1 likely pathogenic or pathogenic variants.

**Genomics England Research Consortium

Ambrose, J. C.[1]; Arumugam, P.[1]; Bleda, M.[1]; Boardman-Pretty, F.[1,2]; Boustred, C. R.[1]; Brittain, H.[1]; Caulfield, M. J.[1,2]; Chan, G. C.[1]; Fowler, T.[1]; Giess A.[1]; Hamblin, A.[1]; Henderson, S.[1,2]; Hubbard, T. J. P.[1]; Jackson, R.[1]; Jones, L. J.[1,2]; Kasperaviciute, D.[1,2]; Kayikci, M.[1]; Kousathanas, A.[1]; Lahnstein, L.[1]; Leigh, S. E. A.[1]; Leong, I. U. S.[1]; Lopez, F. J.[1]; Maleady-Crowe, F.[1]; Moutsianas, L.[1,2]; Mueller, M.[1,2]; Murugaesu, N.[1]; Need, A. C.[1,2]; O'Donovan P.[1]; Odhams, C. A.[1]; Patch, C.[1,2]; Perez-Gil, D.[1]; Pereira, M. B.[1]; Pullinger, J.[1]; Rahim, T.[1]; Rendon, A.[1]; Rogers, T.[1]; Savage, K.[1]; Sawant, K.[1]; Scott, R. H.[1]; Siddiq, A.[1]; Sieghart, A.[1]; Smith, S. C.[1]; Sosinsky, A.[1,2]; Stuckey, A.[1]; Tanguy M.[1]; Thomas, E. R. A.[1,2]; Thompson, S. R.[1]; Tucci, A.[1,2]; Walsh, E.[1]; Welland, M. J.[1]; Williams, E.[1]; Witkowska, K.[1,2]; Wood, S. M.[1,2].

1. Genomics England, London, UK

2. William Harvey Research Institute, Queen Mary University of London, London, EC1M 6BQ, UK.

✉ gaurav-varshney@omrf.org.

#These authors contributed equally: Sheng-Jia Lin, Barbara Vona, Patricia G. Barbalho.

Author Contributions

Conceptualization: S.J.L., B.V., R.M., M.S.Z., V.S., F.A., J.G.G., G.K.V. Data curation: B.V., R.K., R.M., M.S., P.B., A.A., A.T.P., G.A., J.I.E.V., H.A.D.H., N.M., A.O., J.T., D.L.R., J.M., T.S., A.R., M.S.Z., G.K.V. Formal Analysis: S.J.L., B.V., P.G.B., R.K., C.P., M.S., V.S., P.V., P.B., F.A.l., A.T.P., N.M., J.M., L.S.P., D.V.R., E.T., H.Z.E., S.M., T.B.P., H.Y., J.D.W., M.B., B.F., S.K.N. Funding acquisition: B.V., J.G.G., G.K.V. Investigation: A.O., J.T., D.L.R., T.S., B.T., H.G., F.A.l., F.A.S., A.S., K.S., M.G.H., M.K., J.L.M., H.H., E.G.K., F.S.A., T.H., M.S.Z., J.G.G. Project administration: G.K.V. Resources: G.E.R.C. Supervision: B.V., M.G.H., M.K., H.H., F.S.A., T.H., J.G.G., G.K.V. Validation: B.V., R.K., R.M., M.S., P.B., G.A., J.I.E.V., H.A.D.H., N.M., A.O., J.T., D.V.R., A.R., E.T., M.S.Z. Visualization S.D., M.J. Writing – original draft: S.J.L., G.V., B.V., M.S.Z., P.G.B., V.S., M.J., and M.S., Writing – review & editing: S.M.B.

Competing Interests

HZE, TBP, ET, SM, and HY are employees of GeneDx, Inc. All other authors declare no competing interests.

Ethics Declaration

Informed written consent including use of pictures and videos was obtained prior to study inclusion. This study was performed under the tenets of the Declaration of Helsinki and approved by the Ethics Commission of the University of Wuerzburg (46/15), University of Tübingen (197/2019BO01), and University of California San Diego (140028). All experimental animal care was performed in accordance with institutional and NIH guidelines and regulations. The study protocol was approved by the Institutional Animal Care and Use Committee of Oklahoma Medical Research Foundation, protocol 17–02.

Sequencing approaches ranged from disease-specific panels to genome sequencing. We generated loss of function alleles in zebrafish.

Results: We identify ten new and four known biallelic missense variants in *KARS1* presenting with a moderate-to-severe developmental delay, progressive neurological and neurosensory abnormalities, and variable white matter involvement. We describe novel KARS1-associated signs such as autism, hyperactive behavior, pontine hypoplasia, and cerebellar atrophy with prevalent vermian involvement. Loss of *kars1* leads to upregulation of p53, tissue-specific apoptosis, and downregulation of neurodevelopmental related genes, recapitulating key tissue-specific disease phenotypes of patients. Inhibition of p53 rescued several defects of *kars1*$^{-/-}$ knockouts.

Conclusions: Our work delineates the clinical spectrum associated with KARS1 defects and provides a novel animal model for KARS1-related human diseases revealing p53 signaling components as potential therapeutic targets.

INTRODUCTION

Aminoacyl-tRNA synthetases (ARSs) are ubiquitously expressed and essential enzymes required for the aminoacylation of specific amino acids onto their cognate tRNAs. Biallelic variants in ARS genes have been shown to cause a variety of severe and early-onset human diseases[1]. These diseases appear with diverse clinical manifestations such as Charcot-Marie-Tooth disease[2], leukodystrophies[1,3–5], cardiomyopathies[6], hearing loss[7] and other CNS-related pathologies[8–11]. ARS variants can lead to reduced aminoacylation activity, decreased translation accuracy and defects in non-canonical processes[1], but the underlying mechanisms leading to pathology remain poorly understood[12]. As a result, there are no effective treatment strategies for these pathologies.

Of the 37 ARS genes in humans, 18 encode cytoplasmic enzymes, 17 encode mitochondrial enzymes, and two encode bifunctional enzymes; KARS1 (lysyl-tRNA synthetase) is one of the bifunctional ARS enzymes. In humans, a single *KARS1* gene (MIM 601421)[13] encodes both the cytoplasmic and mitochondrial lysyl-tRNA synthetases, which are generated by alternative splicing. Biallelic variants in *KARS1* have been reported in patients with a broad spectrum of clinical manifestations including Charcot-Marie-Tooth[2], non-syndromic hearing loss[14,15], peripheral neuropathy[2], congenital visual impairment[16], progressive microcephaly[16], hypertrophic cardiomyopathy[17], leukoencephalopathies[15,18,19], leukodystrophy[20] and severe neurological and neurosensory disease with optic neuropathy[21]. Twenty-eight pathogenic variants in 30 affected individuals from 25 families have been identified to date, following an autosomal recessive inheritance pattern.

Here, we report 10 new and 4 known biallelic missense variants in *KARS1* in 22 affected individuals from 16 unrelated families. Having included data from 30 previously published *KARS1* cases, we provide a cumulative and comprehensive phenotypic characterization of 52 affected individuals. A mouse knockout of *Kars1* is embryonic lethal and dies before organogenesis occurs[22]. Nevertheless, the function of Kars1 in specific tissues *in vivo* remained unknown. Here, we generated loss of function alleles in zebrafish using CRISPR/Cas9 to understand the function of *kars1 in vivo*.

Materials and Methods

Genetic and phenotypic analysis

Blood samples were collected from all participants and genomic DNA was extracted using standard methods. Sequencing methods and genetic analysis summaries per individual sequenced in each family are summarized in Table S1. Clinical information was collected using standardized templates and completed by collaborating geneticists and clinicians. Brain MRI/CT images from all previously published reports and our cohort were systematically analyzed by a pediatric neuroradiologist. Detailed clinical methods are described in supplementary information.

Zebrafish Functional Studies

Zebrafish (*Danio rerio*) were raised and maintained in an AALAC accredited facility at the Oklahoma Medical Research Foundation (OMRF) under standard conditions, and all experiments were performed as per protocol 17–01 approved by the Institutional Animal Care Committee of OMRF (IACUC). All zebrafish work was carried out in wild-type strain NHGRI-1. Detailed methods related to zebrafish work are described in supplementary methods.

Statistical analysis

Each experiment was repeated three-times, and sample sizes are described in the Supplementary Information. Data are presented as mean value ± standard deviation (SD). Statistical analysis was performed using GraphPad Prism version 8.4 (GraphPad Software, San Diego, CA, USA). In all analyses, the significance level was set to 0.05. The *p*-value was determined as follows: The larval survival curve (Kaplan-Meier representation) was assessed using the Log Rank Mantel-Cox test. One-way ANOVA with Tukey's multiple comparisons test for eye and head size comparisons. Two-tailed unpaired Student's *t*-test with nonparametric Mann-Whitney test for hair cell and motor exon diameter calculation. Two-tailed unpaired Student's *t*-test for the comparison of gene expression levels between two groups, and Holm-Šídák multiple comparisons correction is for multiple groups comparison. Two-tailed unpaired *t*-test with Welch's correction was used for the VSR and auditory evoked behavior response (AEBR) analyses.

Results

Patients with *KARS1* variants show multisystem abnormalities primarily involving the nervous system

We investigated 22 affected individuals from 16 unrelated families who harbored biallelic *KARS1* variants (Fig. 1a). Clinical summaries and variant details are presented in the Case Reports in Supplementary information, Table 1, Figure 1C, and Tables S2 and S3. All patients underwent either exome, genome or targeted gene sequencing and analyses, which excluded other functionally relevant variants compatible with Mendelian diseases, based on mode of inheritance and clinical presentation. Variants were Sanger sequence-confirmed (Fig. S1). We identified 10 previously unpublished variants and four previously reported variants[18,19,21,23,24] as listed in Table 1, and Figure S2. Each substitution affected

a conserved amino acid, and all the variants are predicted to be deleterious (Supplementary information, Fig. S3).

Clinical description

The cohort mostly presented with a moderate-to-severe developmental delay, progressive neurological and neurosensory impairment, and white matter involvement, variably associated with developmental regression, intellectual disability, behavioral abnormalities, and additional extra neurological signs. The disease typically manifested during early childhood with developmental delay and/or hearing impairment. Developmental regression was reported in 7/22 cases (32%). Four cases died at the mean age of 13.9 years due to respiratory infection (2/4), sepsis (1/4) or post-febrile illness associated with severe deterioration (1/4). All parents were asymptomatic and did not exhibit neurological symptoms. Developmental delay was present in 86% of cases (19/22) followed by intellectual disability (15/21, 71%), speech delay (11/19, 58%), absent speech (11/20, 55%), failure to thrive (4/22, 18%), and behavioral abnormalities such as autism (3/21, 14%), and hyperactive behavior (6/21, 29%).

All cases uniformly expressed neurological symptoms (22/22, 100%), frequently involving sensorineural hearing loss (20/21, 95%), seizures (13/22, 59%), hypotonia (9/22, 41%), cerebellar ataxia (7/22, 32%), spasticity (8/22, 36%), strabismus (6/20, 30%) and nystagmus (4/20, 20%), and acquired joint contractures (4/22,18%). Hearing loss was severe-to-profound in 16/21 cases (76%), and 5/10 (50%) of them had cochlear implants. Other variable neurological features included visual impairment/optic atrophy (7/20, 35%), quadriplegia (3/22, 14%), dystonia and tremor (2/22, 9%), neuropathy (1/10, 10%), neurophysiologically confirmed skeletal myopathy (2/22, 9%) (Video S1–2), generalized muscle atrophy (2/22, 9%), and incontinence (4/22, 18%). None of the cases expressed isolated hearing loss or sensory-motor neuropathy as the main clinical feature.

While not every case was uniformly examined, roughly half were clinically diagnosed with microcephaly (10/18, 56%). Interestingly, dysmorphic facial features were common in 67% (14/21) of the cohort and this included a high or narrow forehead, prominent nose, short philtrum, low-set ears, broad nasal bridge, thin upper lip, epicanthus, and telecanthus (Fig. 1b; Supplementary Case Report includes detailed descriptions). Other extra-neurological signs included feeding difficulties (6/22, 27%), and neonatal vomiting with diarrhea (2/22, 11%). Single isolated cases displayed hypertrophic cardiomyopathy (1/11, 9%), and neonatal vomiting with diarrhea (2/22, 11%). The case with hypertrophic cardiomyopathy did not have available levels of lactate and mitochondrial respiratory chain enzymes measured.

Neuroimaging findings

Brain MRI studies were available for 21/22 (95%) individuals (with more than one examination in 2 cases), while head CT and spinal MRI were available for three and one subjects, respectively (Fig. 1d–o). White matter involvement was noted in 13/21 (61.9%) individuals. In 5/13 (38.4%) subjects, there were confluent T2 hyperintensities in the periventricular white matter, with prevalent involvement of parieto-occipital regions; one

of these subjects studied at 53 years of age had a previous normal brain MRI (performed 8 years before). In 4/13 (23%) subjects, there was mild diffuse T2 hyperintensity of the supratentorial white matter, with sparing of the corpus callosum and U fibers; one of these individuals studied at 4 years of age had a previous normal brain MRI (performed 2 years before). Two subjects (2/13, 15.3%) presented diffuse leukodystrophy with corpus callosum involvement, sparing of the U fibers, and calcifications; in one of them the cerebellar white matter was also involved. Delayed myelination was noted in 2 other subjects (2/13, 15.3%). White matter volume loss with ventricular enlargement was present in 10/21 (47.6%) cases. Enlargement of the cerebral CSF spaces, mainly in the fronto-temporal regions was observed in 9/21 (42.8%) individuals. Hypoplasia of the pons and corpus callosum was noted in 7/21 (33.3%) and 6/21 (28.5%) of cases, respectively. Cerebellar atrophy, with prevalent or isolated vermian involvement was noted in 5/21 (23.8%) of cases. Finally, in 4/21 (19%) subjects, the brain MRI was normal.

Genotype-phenotype correlation

Inter- and intrafamilial phenotypic variability was noticed among individuals with the same variants in the present *KARS1* cohort. For instance, three affected siblings in Family 11 each harbored a homozygous *KARS1* c.379T>C (p.(Phe127Leu)) variant, and although they shared common symptoms such as developmental delay, infantile-onset profound hearing loss, dysmorphic facial features, spasticity, and varying degree of joint contractures, several important symptoms were expressed only by one of them. This included regression, epilepsy, optic atrophy, failure to thrive, and hyperactivity. The same *KARS1* variant was homozygous in the proband from Family 1, who differed from Family 11 by a preserved vision, cerebellar ataxia, classic leukodystrophy on MRI, and the basal ganglia calcification. Similarly, 5 affected members from three independent families were homozygous for the *KARS1* c.1772A>T (p.(Asn591Ile)) variant and they had variable intra- and interfamilial expression of epileptic seizures, cerebellar ataxia, intellectual disability, hypotonia, polyneuropathy, behavioral abnormalities, and impaired speech. Significant phenotypic variability was also noticed between families 9 and 15 harboring the similar compound heterozygous *KARS1* variants c.683C>T (p.(Pro228Leu)) and c.774A>T (p.(Arg258Ser)).

kars1 zebrafish disease model using CRISPR/Cas9-mediated targeted mutagenesis.

Zebrafish has a single *kars1* gene (NCBI Gene ID: 280647) generating two transcript variants via alternative RNA splicing, confirmed by RT-PCR from multiple developmental stages (Fig. S4, and Supplementary information). To unravel the function of KARS1, we examined *kars1* mRNA expression in zebrafish embryonic development using whole-mount *in situ* hybridization (WISH). *kars1* mRNA was initially ubiquitously expressed but gradually became more prominent in the central nervous system (CNS), eye, inner ear, muscles, and digestive system (liver, intestine and pancreas) (Fig. 2a–c, Supplementary information, and Fig. S5a–g). We generated *kars1* loss-of-function zebrafish mutant lines using CRISPR/Cas9 and identified 3 independent alleles $kars1^{om1del7}$, $kars1^{om2del8}$ and $kars1^{om3del7}$ (Fig.S6 a–d). Homozygous $kars1^{-/-}$ animals showed morphological abnormalities starting at approximately 3 dpf including heart edema (black arrow), as well as smaller heads (blue line), eye (red line) and otic vesicle (red arrowhead) when compared to

WT animals (Fig. 2d and e, and Fig. S7a–c). *Kars1* homozygous larvae also failed to inflate the swim bladder (black arrowhead) and showed abnormal trunk muscle fibers. We observed 100% mortality by 10 dpf for all three *kars1* homozygous mutant larvae, possibly because of the inability to feed (Fig. 2f and Fig. S7d). We quantified the eye and head axial length which were significantly reduced in *kars1*$^{-/-}$ mutants compared to control animals (Fig. 2g and h). Additionally, the *kars1*$^{-/-}$ larvae failed to respond to touch and displayed a loss of spatial orientation (Fig. S7e, f and Video S3). The side-laying position observed in *kars1*$^{-/-}$ mutant larvae might reflect loss of vestibular function, severe muscle control failure, and/or absence of an inflated swim bladder which all affect balance. Given the *kars1*$^{-/-}$ mutants showed morphological defects in the eyes and ears, and failed to response to touch, we further quantified their visual startle response (VSR) and AEBR, *kars1*$^{-/-}$ mutants showed completed loss of locomotor activity in response to light or acoustic startle (Fig. 2i and j). Overall, the tissue/organ-specific morphological defects in *kars1*$^{-/-}$ mutants found in the eye, inner ear, and trunk muscles appeared to directly correlate with *kars1* mRNA expression patterns during embryo development, strongly suggesting these phenotypes and behaviors arose from Kars1 loss-of-function.

To confirm the phenotypes of the *kars1*$^{-/-}$ mutant animals arise from loss of *kars1* function, we performed mRNA rescue experiments by injecting either human WT *KARS1* or the zebrafish WT *kars1* mRNA. Co-injection of mRNAs encoding the mitochondrial and cytoplasmic isoforms into 1-cell stage showed reduced frequencies of heart edema (Fig. 2k) and significantly restored eye size in *kars1*$^{-/-}$ mutants (Fig. 2l). Furthermore, microinjection of zebrafish *kars1* mRNA further rescued the startle responses compared to *kars1*$^{-/-}$ mutant animals (Fig. 2m and n) suggesting mutant phenotypes are caused by *kars1* loss-of-function.

The *kars1* loss-of-function zebrafish model recapitulates patient symptoms.

Histological analysis of the brain of 5 dpf larvae revealed a vacuolated spongiosus appearance with areas of reduced cell density and disorganized segment boundaries in *kars1*$^{-/-}$ mutants compared to WT siblings (Fig. 3a–c). Moreover, eye volume was reduced and the retinal layer organization was completely lost in the *kars1*$^{-/-}$ mutants compared to WT siblings (Fig. 3b) strongly suggesting impaired vision. Furthermore, the number of neuronal cells appeared strongly reduced in the brain and retina in *kars1*$^{-/-}$ mutants compared to controls (Fig. 3a and b). Immunohistochemical analysis of neuronal synapses revealed reduced staining in all brain and eye regions pointing to a significant reduction of synapses in *kars1*$^{-/-}$ mutants (Fig. 3d), suggesting impaired neuronal transmission. Additionally, staining revealed abnormal motor neuron morphology, including shrinkage of motor neuron axon projections and reduction of terminal axonal branching in the mutants (Fig. 3e), further indicating strong alteration of locomotor function in those animals.

Individuals with biallelic *KARS1* pathogenic variants usually present with combined neuronal and muscular dysfunction. Indeed, our WISH data revealed *kars1* mRNA expression in trunk muscles (Fig. 2a) and a loss of touch-evoked responses in the *kars1*$^{-/-}$ mutants (Fig. S7e and Video S3). Phalloidin staining that labels actins showed weaker staining in the myotomes and presented misaligned and detached muscle fibers from the

myotendinous junction (MTJ) (Fig. 3f and g) suggesting severe neuromuscular dysfunction leading to absence of coordinated locomotion.

Several individuals with *KARS1* variant alleles also display hearing disorders reminiscent of the inner ear defects observed in *kars1*$^{-/-}$ mutant larvae, such as perturbed sensory epithelia and loss of AEBR startle response. Morphological analysis of the mutants showed smaller otic vesicles and otoliths (Fig. 3h) and flattened sensory epithelia in both anterior and posterior maculae (Fig. 3c). The phalloidin staining in the inner ear showed strong reduction in the number of F-actin-rich stereocilia, which are crucial for the formation of hair cell bundles and thus for mechanoelectrical transduction (Fig. 3i). Vital stain Yo-PRO-1 iodide, showed fewer hair cells in the zebrafish lateral line which are morphologically and functionally similar to those of the inner ear[25] (Fig. S8a and b). Taken together, these findings suggest that *kars1* plays a crucial role in hair cell formation in zebrafish, reminiscent of hearing disorders found in a subset of individuals affected with *KARS1* variants.

Variants in *KARS1* have been shown to be associated with seizures (Table S2). Seizure activity positively correlates with the expression of *c-fos* (*fosab* in zebrafish), a marker for general neuronal activity. We used classical pro-chemoconvulsant drug pentylenetetrazol (PTZ) to induce seizure activity and elevated expression of *fosab* mRNA (Fig. S8c). Intriguingly, untreated *kars1*$^{-/-}$ larvae, when compared with untreated WT controls, exhibited two-fold at 3 dpf and ten-fold increase in *fosab* mRNA levels (Fig. S8d) suggesting seizure-like activity in homozygous animals.

Together, our morphological, behavioral and histological analyses demonstrate that the *kars1*$^{-/-}$ zebrafish mutant larvae exhibit visual impairment, neuromuscular dysfunction, sensorineural hearing loss, and increased expression of seizure marker, *c-fos*, thus recapitulating a number of pathologies found in individuals with *KARS1* variants.

Kars1 loss-of-function triggers p53-mediated apoptosis and downregulation of key neurodevelopmental related genes

To determine the consequences of Kars1 loss-of-function on gene expression, we performed RNA-sequencing (RNA-Seq) on WT and *kars1*$^{-/-}$ mutants at 3 dpf and 4 dpf and compared gene expression profiles. We found 1,616 and 1,409 differentially expressed genes (DEGs) at 3 dpf and 4 dpf respectively, 563 genes overlapped between 3 dpf and 4 dpf (Fig. S9a–c, and Table S5). KEGG pathway analysis showed *kars1* loss-of-function dysregulated many pathways including the p53 and cell apoptosis pathway (Fig. S10–12). ARSs have been shown to regulate cell death pathways[26,27]. To test whether the morphological defects found in *kars1*$^{-/-}$ mutants were due to abnormal cell apoptosis, we performed a TUNEL assay and observed an increase in TUNEL-positive cells in the brain, eye, trunk and inner ear of *kars1*$^{-/-}$ mutants compared with sibling animals at 5 dpf (Fig. S13a and b), suggesting distinct cell types are particularly sensitive to loss of Kars1. Next, to determine whether increased cell apoptosis was mediated by p53 activation, we knocked down *tp53* by microinjecting *kars1*$^{-/-}$ mutant animals with *tp53* anti-sense morpholinos (MO) and subsequently performed the TUNEL assays at 3 dpf. Results showed a significant reduction in the TUNEL-positive signals in the brain, eye, ear and trunk in the MO-injected *kars1*$^{-/-}$

mutant (Fig. 4a–c). Strikingly, reduction in eye size (Fig. 4d), and up-regulation of several apoptosis markers were restored to WT levels (Fig. 4e), therefore confirming the p53 pathway was successfully knocked down, and furthermore implicating it in reduction of eye size. To further characterize the functional rescue at the molecular level after inhibiting the p53 pathway, we examined the expression of six genes we previously found to be downregulated in *kars1*$^{-/-}$ mutants (Fig. 4f). All six genes showed at least partially restored expression upon p53 knockdown in *kars1*$^{-/-}$ mutants. Taken together, the loss of Kars1 upregulated the p53 pathway thus leading to apoptosis thereby causing multiple phenotypic abnormalities.

To validate our findings, we used CRISPR/Cas9 technology to generate biallelic variants. Co-injecting WT *kars1* mRNAs with the *kars1* sgRNAs rescued these phenotypes, confirming they arise from Kars1 loss-of-function (Fig. 4g). Importantly, co-injection of *tp53* sgRNAs with *kars1* sgRNAs restored the eye and head size of the *kars1* F_0 mutants (Fig. 4g–i). Moreover, whereas 90% of *kars1* F_0 mutant animals died by 10 dpf, only 20% of animals co-injected with either *kars1* mRNAs or *tp53* sgRNAs died by 10 dpf (Fig. 4j). Histological analysis showed vacuolated spongiosus appearance in the brain was significantly restored in *kars1;tp53* F_0 mutants compared to *kars1* F_0 mutants, as was eye volume and retinal layer organization (Fig. 4k) and vision/hearing startle responses (Fig. S13c and d). At the molecular level, *kars1* F_0 mutants showed significantly reduced *kars1* expression and increased *tp53* expression compared to the uninjected control, whereas *kars1;tp53* F_0 mutants showed significantly reduced expression of both *kars1* and *tp53* (Fig. S13e). Additionally, *kars1* F_0 mutants showed increased *casp8* and decreased *mbpa*, *neurod1* and *stxbp1a* expression compared to controls that was restored in *kars1;tp53* F_0 mutants (Fig. S13f). Together, our results showed *kars1* F_0 mutants phenocopy the *kars1*$^{-/-}$ mutant, and p53 depletion mitigates the morphological, behavior, and molecular phenotypes due to loss of Kars1.

Discussion

Deciphering how variants in different ARS genes cause diverse organ-specific phenotypes is crucial to inform therapeutic approaches for ARS-related disorders. We report 10 novel and four known variants in *KARS1* from 22 patients belonging to 16 unrelated families. Having included the clinical and neuroimaging data from our cohort and the corresponding data from the previously published 30 *KARS1* cases (25 families), we made a cumulative phenotypic characterization for 52 cases with biallelic *KARS1* variants (Fig. 1c).

Notably, our cohort expands the phenotypic spectrum of *KARS1* variants to include autism/hyperactivity. Additionally, we highlight a variety of *KARS1*-associated dysmorphic facial features, as facial dysmorphism has rarely been described in previous *KARS1* reports. It is reported in 11/52 individuals, where 10 cases were identified in our cohort and 1 case from McLaughlin *et al*[2]. We also provide further supporting evidence for skeletal myopathy, a phenotype that has previously been reported in one case[17]. Our case with hypertrophic cardiomyopathy (Family 4) seems to also highlight the importance of this phenotype as in the previous few reports[17,28]. Finally, we highlight cerebellar ataxia might be a frequent *KARS1*-associated feature that was previously reported only in 3/30 (10%) cases but present

in 32% (7/22) of our cohort. Our cumulative phenotypic analysis showed that similar to other ARSs, *KARS1* expresses predominant neurological and neurosensory phenotypes associated with facial dysmorphism[29].

The systematic analysis of all available neuroimaging data, including the present cases, suggests the spectrum of manifestations associated with *KARS1* variants is wide, ranging from normal brain appearance to a severe leukodystrophy with rapid brain atrophy. Slightly more than one third of cases (18/52, 34.6%) presented with a progressive leukodystrophy, involving the corpus callosum and sparing the U fibers, variably extending to the spinal cord and cerebellar white matter, often associated with peculiar cerebral and spinal cord calcifications[18–20]. Less specific patterns included faint diffuse (6/52, 11.5%) or multifocal periventricular (7/52, 13.4%) white matter signal alterations. Interestingly, a third of the present patients had callosal hypoplasia, a likely underestimated feature previously described in three subjects with *KARS1* variants[16,30]. This finding is only partly related to the loss of cerebral white matter volume, as the corpus callosum in these subjects is thin but also shorter than normal. In addition, we uncovered hypoplasia of the pons in one third of subjects, and atrophy of cerebellum with prevalent vermian involvement in 20% of cases. Taken together, these neuroimaging features expand the phenotypes related to *KARS1* variants, indicating a prenatal onset of the disease often associated with a rapid neurodegenerative course[31,32].

Although a clear genotype-phenotype correlation in *KARS1*-related disease is lacking, we noticed some interesting associations. The *KARS1* c.379T>C (p.(Phe127Leu)) variant was present in the case from Family 1 in a homozygous state, and the same variant was present in compound heterozygosity in one of the cases from the Ardissone *et al.* report[18]. Besides the typical developmental delay and hearing loss, both cases shared other phenotypic similarity including seizures, psychomotor regression, hypotonia, spastic tetraparesis, and brain calcifications. The *KARS1* c.683C>T (p.(Pro228Leu)) variant was present in compound heterozygosity in Family 9 and a report by Scheidecker *et al.*[21], and both families manifested ataxia, visual impairment, and dystonia. Identifying and characterizing homozygous individuals with these variants in the future would be of interest to further evaluate this potential association.

Biallelic *KARS1* variants have emerged as a cause of rare early-onset childhood neurodegenerative disorders presenting with a multiorgan dysfunction suggestive of mitochondrial disorders but usually with normal biochemical assays. Therefore, in addition to the initial association of biallelic *KARS1* variants with Charcot-Marie-Tooth disease and non-syndromic hearing loss in single isolated cases (2/50), an early-onset complex neurological and syndromic phenotype should be assigned to *KARS1* in an Online Catalog of Human Genes and Genetic Disorders (OMIM). This might yield more families with *KARS1*-related disease and improve understanding of its neurobiology and phenotypic spectrum.

The physiological relevance of several ARS genes has been assessed *in vivo* using zebrafish[33,34,35]. Here, we showed *kars1* homozygous (*kars1*$^{-/-}$) zebrafish larvae exhibit the phenotypic hallmarks associated with pathogenic variants reported in patients. In agreement

with our study, *Kars1* knockdown in *Xenopus* caused developmental defects of head and eyes; loss of myelination and reduced expression of myelin binding protein, leading to incomplete formation of white matter, and reduced brain volume suggesting an important role of KARS1 across the species[20].

Loss of ARS enzymes have been shown to activate the p53 signaling pathway[36]. Likewise, in zebrafish, overexpression of an editing-defective valyl-tRNA synthetase (VARS1) activates the p53 signaling pathway, and increased expression of targets such as cyclin-dependent kinase inhibitor p21 (*cdkn1a*) and *gadd45* leading to cell death[37]. *Kars1*$^{-/-}$ mutants show upregulation of p53 signaling and apoptosis pathway genes. Interestingly, up-regulation of p53 signaling has been connected to apoptosis of human oligodendrocytes (a type of myelin-forming cells)[38], and cuprizone-[39] or compressed spinal cord injury-[40] induced demyelination (one of the categories in leukodystrophy classification) in mice. Genetic or pharmacological inhibition of p53 decreased the susceptibility of cuprizone-induced demyelination and increased the survival rate of oligodendrocytes[39]. These data and our current findings emphasize that p53 pathway inhibitors might represent potential therapeutics for KARS1 patients.

One of the limitation of this study is lack of functional variant analysis in zebrafish. However, our structural modeling data shows 27/36 variants occur in the aminoacylation domain, therefore, likely affect enzyme activity. Since KARS1 is a multifunctional protein, variants in this study could affect the canonical as well as noncanonical functions of the protein.

In summary, our findings underscore a conserved and unique requirement for ARS during nervous system and muscle development to prevent p53-mediated apoptosis and disease. Our disease model offers promising avenues to explore the biallelic contributions of KARS1, and similar approaches could be exploited to understand a number of diseases associated with variants in essential genes.

Supplementary Material

Refer to Web version on PubMed Central for supplementary material.

Authors

Sheng-Jia Lin[#,1], Barbara Vona[#,2,3], Patricia G Barbalho[#,1], Rauan Kaiyrzhanov[4], Reza Maroofian[4], Cassidy Petree[1], Mariasavina Severino[5], Valentina Stanley[6], Pratishtha Varshney[1], Paulina Bahena[3], Fatema Alzahrani[7], Amal Alhashem[8], Alistair T Pagnamenta[9], Gudrun Aubertin[10], Juvianee I Estrada-Veras[11,12,13], Héctor Adrián Díaz Hernández[14], Neda Mazaheri[15,16], Andrea Oza[17], Jenny Thies[18], Deborah L Renaud[19], Sanmati Dugad[20], Jennifer McEvoy[6], Tipu Sultan[21], Lynn S Pais[22], Brahim Tabarki[8], Daniel Villalobos-Ramirez[23], Aboulfazl Rad[2], Genomics England Research Consortium[**], Hamid Galehdari[14], Farah Ashrafzadeh[24], Afsaneh Sahebzamani[25], Kolsoum Saeidi[26], Erin Torti[27], Houda Z Elloumi[27], Sara Mora[27], Timothy B Palculict[27], Hui Yang[27], Jonathan D Wren[1], Ben Fowler[28], Manali Joshi[20], Martine Behra[29], Shawn M Burgess[30], Swapan K

Nath[31], Michael G Hanna[4], Margaret Kenna[17], J Lawrence Merritt 2nd[32], Henry Houlden[4], Ehsan Ghayoor Karimiani[33,34], Maha S Zaki[35], Thomas Haaf[3], Fowzan S Alkuraya[7,8], Joseph G Gleeson[6], Gaurav K Varshney[1]

Affiliations

[1.] Genes & Human Disease Research Program, Oklahoma Medical Research Foundation, Oklahoma City, OK, USA.

[2.] Department of Otolaryngology–Head & Neck Surgery, Tübingen Hearing Research Centre, Eberhard Karls University of Tübingen, Tübingen, Germany.

[3.] Institute of Human Genetics, Julius Maximilians University Würzburg, Würzburg, Germany.

[4.] Department of Neuromuscular Disorders, Queen Square Institute of Neurology, University College London, London, UK.

[5.] Neuroradiology Unit, IRCCS Istituto Giannina Gaslini, Genoa, Italy.

[6.] Department of Neurosciences, Rady Children's Institute for Genomic Medicine, University of California San Diego, La Jolla, CA, USA.

[7.] Department of Genetics, King Faisal Specialist Hospital and Research Center, Riyadh, Saudi Arabia.

[8.] Department of Pediatrics, Prince Sultan Military Medical City, Riyadh, Saudi Arabia.

[9.] NIHR Biomedical Research Centre, Wellcome Centre for Human Genetics, University of Oxford, Oxford, UK.

[10.] Division of Medical Genetics, Department of Pathology and Lab Medicine, Island Health, Victoria General Hospital, Victoria, BC, Canada.

[11.] Henry M Jackson Foundation for the Advancement of Military Medicine, Bethesda, MD, USA.

[12.] Pediatric Subspecialty Genetics Walter Reed National Military Medical Center, Bethesda, MD, USA.

[13.] Murtha Cancer Center / Research Program, Department of Surgery, Uniformed Services University of the Health Sciences, Bethesda, MD, USA.

[14.] Department of Gastrointestinal Endoscopy, National Institute of Medical Sciences and Nutrition Salvador Zubirán, Mexico City, Mexico.

[15.] Department of Genetics, Faculty of Science, Shahid Chamran University of Ahvaz, Ahvaz, Iran.

[16.] Narges Medical Genetics and Prenatal Diagnostics Laboratory, East Mihan Ave., Kianpars, Iran.

[17.] Otolaryngology and Communication Enhancement, Boston Children's Hospital, and Dept. of Otolaryngology, Harvard medical School, Boston, USA.

[18.] Department of Biochemical Genetics, Seattle Children's Hospital, Seattle, WA, USA.

[19.] Departments of Neurology and Pediatrics, Mayo Clinic College of Medicine and Science, Rochester, MN, USA.

[20.] Bioinformatics Centre, S. P. Pune University, Pune, India.

[21.] Department of Pediatric Neurology, Children's Hospital and Institute of Child Health, Lahore, Pakistan.

[22.] Broad Center for Mendelian Genomics, Program in Medical and Population Genetics, Broad Institute of Massachusetts Institute of Technology and Harvard, Cambridge, MA, USA.

[23.] Department of Bioinformatics, Biocenter, University of Würzburg, Würzburg, Germany.

[24.] Department of Pediatric Diseases, Mashhad University of Medical Sciences, Mashhad, Iran.

[25.] Pediatric and Genetic Counselling Center, Kerman Welfare Organization, Kerman, Iran.

[26.] Neuroscience Research Center, Institute of Neuropharmacology, Kerman University of Medical Sciences, Kerman, Iran.

[27.] GeneDx, 207 Perry Parkway Gaithersburg, Gaithersburg, MD, USA.

[28.] Imaging core facility, Oklahoma Medical Research Foundation, Oklahoma City, OK, USA.

[29.] Department of Neurobiology, University of Puerto Rico, San Juan, PR, USA.

[30.] Translational & Functional Genomics Branch, National Human Genome Research Institute, NIH, Bethesda, MD, USA.

[31.] Arthritis & Clinical Immunology Research Program, Oklahoma Medical Research Foundation, Oklahoma City, OK, USA.

[32.] Department of Pediatrics, Biochemical Genetics, University of Washington, Seattle, WA, USA.

[33.] Molecular and Clinical Sciences Institute, St. George's, University of London, Cranmer Terrace London, London, UK.

[34.] Innovative Medical Research Center, Mashhad Branch, Islamic Azdad University, Mashhad, Iran.

[35.] Clinical Genetics Department, Human Genetics and Genome Research Division, National Research Centre, Cairo, Egypt.

Acknowledgements

This research is supported by a grant from NIH GM103636 (Project 3), and the Presbyterian Health Foundation (PHF) (GKV), NIH grants, R01NS048453, R01NS052455 (J.G.G.), Intramural Funding (*f*ortüne) at the University

of Tübingen (2545-1-0 to B.V.) and the Ministry of Science, Research and Art Baden-Württemberg (to B.V.). Sequencing and analysis were provided by the Broad Institute (UM1 HG008900, R01HG009141) & Yale Center for Mendelian Disorders (U54HG006504 to M. Gunel). This research was made possible in part through the 100,000 Genomes Project, UK.

Data Availability

Human variant data included in this study have been deposited in Leiden Open Variation Database (LOVD) and available through following accession numbers: 0000685774 (https://databases.lovd.nl/shared/variants/0000685774), 0000685798 (https://databases.lovd.nl/shared/variants/0000685798), 0000685800 (https://databases.lovd.nl/shared/variants/0000685800), 0000685801 (https://databases.lovd.nl/shared/variants/0000685801), 0000685802 (https://databases.lovd.nl/shared/variants/0000685802), 0000685803 (https://databases.lovd.nl/shared/variants/0000685803), 0000685804 (https://databases.lovd.nl/shared/variants/0000685804), 0000685805 (https://databases.lovd.nl/shared/variants/0000685805). Reagents related to zebrafish experiments described in this manuscript are available upon request.

References

1. Meyer-Schuman R, Antonellis A. Emerging mechanisms of aminoacyl-tRNA synthetase mutations in recessive and dominant human disease. Hum Mol Genet. 2017;26(R2):R114–R127. [PubMed: 28633377]
2. McLaughlin HM, Sakaguchi R, Liu C, et al. Compound heterozygosity for loss-of-function lysyl-tRNA synthetase mutations in a patient with peripheral neuropathy. Am J Hum Genet. 2010;87(4):560–566. [PubMed: 20920668]
3. Scheper GC, van der Klok T, van Andel RJ, et al. Mitochondrial aspartyl-tRNA synthetase deficiency causes leukoencephalopathy with brain stem and spinal cord involvement and lactate elevation. Nat Genet. 2007;39(4):534–539. [PubMed: 17384640]
4. Messmer M, Florentz C, Schwenzer H, et al. A human pathology-related mutation prevents import of an aminoacyl-tRNA synthetase into mitochondria. Biochem J. 2011;433(3):441–446. [PubMed: 21121901]
5. Maffezzini C, Laine I, Dallabona C, et al. Mutations in the mitochondrial tryptophanyl-tRNA synthetase cause growth retardation and progressive leukoencephalopathy. Mol Genet Genomic Med. 2019;7(6):e654. [PubMed: 30920170]
6. Gotz A, Tyynismaa H, Euro L, et al. Exome sequencing identifies mitochondrial alanyl-tRNA synthetase mutations in infantile mitochondrial cardiomyopathy. Am J Hum Genet. 2011;88(5):635–642. [PubMed: 21549344]
7. Almalki A, Alston CL, Parker A, et al. Mutation of the human mitochondrial phenylalanine-tRNA synthetase causes infantile-onset epilepsy and cytochrome c oxidase deficiency. Biochim Biophys Acta. 2014;1842(1):56–64. [PubMed: 24161539]
8. Latour P, Thauvin-Robinet C, Baudelet-Mery C, et al. A major determinant for binding and aminoacylation of tRNA(Ala) in cytoplasmic Alanyl-tRNA synthetase is mutated in dominant axonal Charcot-Marie-Tooth disease. Am J Hum Genet. 2010;86(1):77–82. [PubMed: 20045102]
9. McLaughlin HM, Sakaguchi R, Giblin W, et al. A recurrent loss-of-function alanyl-tRNA synthetase (AARS) mutation in patients with Charcot-Marie-Tooth disease type 2N (CMT2N). Hum Mutat. 2012;33(1):244–253. [PubMed: 22009580]
10. Gonzalez M, McLaughlin H, Houlden H, et al. Exome sequencing identifies a significant variant in methionyl-tRNA synthetase (MARS) in a family with late-onset CMT2. J Neurol Neurosurg Psychiatry. 2013;84(11):1247–1249. [PubMed: 23729695]
11. Safka Brozkova D, Deconinck T, Griffin LB, et al. Loss of function mutations in HARS cause a spectrum of inherited peripheral neuropathies. Brain. 2015;138(Pt 8):2161–2172. [PubMed: 26072516]

12. Oprescu SN, Griffin LB, Beg AA, Antonellis A. Predicting the pathogenicity of aminoacyl-tRNA synthetase mutations. Methods. 2017;113:139–151. [PubMed: 27876679]
13. Tolkunova E, Park H, Xia J, King MP, Davidson E. The human lysyl-tRNA synthetase gene encodes both the cytoplasmic and mitochondrial enzymes by means of an unusual alternative splicing of the primary transcript. J Biol Chem. 2000;275(45):35063–35069. [PubMed: 10952987]
14. Santos-Cortez RL, Lee K, Azeem Z, et al. Mutations in KARS, encoding lysyl-tRNA synthetase, cause autosomal-recessive nonsyndromic hearing impairment DFNB89. Am J Hum Genet. 2013;93(1):132–140. [PubMed: 23768514]
15. Zhou XL, He LX, Yu LJ, et al. Mutations in KARS cause early-onset hearing loss and leukoencephalopathy: Potential pathogenic mechanism. Hum Mutat. 2017;38(12):1740–1750. [PubMed: 28887846]
16. McMillan HJ, Humphreys P, Smith A, et al. Congenital Visual Impairment and Progressive Microcephaly Due to Lysyl-Transfer Ribonucleic Acid (RNA) Synthetase (KARS) Mutations: The Expanding Phenotype of Aminoacyl-Transfer RNA Synthetase Mutations in Human Disease. J Child Neurol. 2015;30(8):1037–1043. [PubMed: 25330800]
17. Verrigni D, Diodato D, Di Nottia M, et al. Novel mutations in KARS cause hypertrophic cardiomyopathy and combined mitochondrial respiratory chain defect. Clin Genet. 2017;91(6):918–923. [PubMed: 27891585]
18. Ardissone A, Tonduti D, Legati A, et al. KARS-related diseases: progressive leukoencephalopathy with brainstem and spinal cord calcifications as new phenotype and a review of literature. Orphanet J Rare Dis. 2018;13(1):45. [PubMed: 29615062]
19. Sun C, Song J, Jiang Y, et al. Loss-of-function mutations in Lysyl-tRNA synthetase cause various leukoencephalopathy phenotypes. Neurol Genet. 2019;5(2):e565. [PubMed: 31192300]
20. Itoh M, Dai H, Horike SI, et al. Biallelic KARS pathogenic variants cause an early-onset progressive leukodystrophy. Brain. 2019;142(3):560–573. [PubMed: 30715177]
21. Scheidecker S, Bär S, Stoetzel C, et al. Mutations in KARS cause a severe neurological and neurosensory disease with optic neuropathy. Hum Mutat. 2019.
22. Dickinson ME, Flenniken AM, Ji X, et al. High-throughput discovery of novel developmental phenotypes. Nature. 2016;537(7621):508–514. [PubMed: 27626380]
23. Murray CR, Abel SN, McClure MB, et al. Novel Causative Variants in DYRK1A, KARS, and KAT6A Associated with Intellectual Disability and Additional Phenotypic Features. J Pediatr Genet. 2017;6(2):77–83. [PubMed: 28496994]
24. Lieber DS, Calvo SE, Shanahan K, et al. Targeted exome sequencing of suspected mitochondrial disorders. Neurology. 2013;80(19):1762–1770. [PubMed: 23596069]
25. Fay RR, Popper AN. Evolution of hearing in vertebrates: the inner ears and processing. Hear Res. 2000;149(1–2):1–10. [PubMed: 11033242]
26. Park SG, Schimmel P, Kim S. Aminoacyl tRNA synthetases and their connections to disease. Proc Natl Acad Sci U S A. 2008;105(32):11043–11049. [PubMed: 18682559]
27. Hyeon DY, Kim JH, Ahn TJ, Cho Y, Hwang D, Kim S. Evolution of the multi-tRNA synthetase complex and its role in cancer. J Biol Chem. 2019;294(14):5340–5351. [PubMed: 30782841]
28. Kohda M, Tokuzawa Y, Kishita Y, et al. A Comprehensive Genomic Analysis Reveals the Genetic Landscape of Mitochondrial Respiratory Chain Complex Deficiencies. PLoS Genet. 2016;12(1):e1005679. [PubMed: 26741492]
29. Fuchs SA, Schene IF, Kok G, et al. Aminoacyl-tRNA synthetase deficiencies in search of common themes. Genet Med. 2019;21(2):319–330. [PubMed: 29875423]
30. Vargas A, Rojas J, Aivasovsky I, et al. Progressive Early-Onset Leukodystrophy Related to Biallelic Variants in the KARS Gene: The First Case Described in Latin America. Genes (Basel). 2020;11(12).
31. Edvardson S, Shaag A, Kolesnikova O, et al. Deleterious mutation in the mitochondrial arginyl-transfer RNA synthetase gene is associated with pontocerebellar hypoplasia. Am J Hum Genet. 2007;81(4):857–862. [PubMed: 17847012]
32. Mendes MI, Green LMC, Bertini E, et al. RARS1-related hypomyelinating leukodystrophy: Expanding the spectrum. Ann Clin Transl Neurol. 2020;7(1):83–93. [PubMed: 31814314]

33. Malissovas N, Griffin LB, Antonellis A, Beis D. Dimerization is required for GARS-mediated neurotoxicity in dominant CMT disease. Hum Mol Genet. 2016;25(8):1528–1542. [PubMed: 27008886]

34. Siekierska A, Stamberger H, Deconinck T, et al. Biallelic VARS variants cause developmental encephalopathy with microcephaly that is recapitulated in vars knockout zebrafish. Nat Commun. 2019;10(1):708. [PubMed: 30755616]

35. Friedman J, Smith DE, Issa MY, et al. Biallelic mutations in valyl-tRNA synthetase gene VARS are associated with a progressive neurodevelopmental epileptic encephalopathy. Nat Commun. 2019;10(1):707. [PubMed: 30755602]

36. Fukushima K, Motomura S, Kuraoka A, Nakano H, Nishimoto T. A single point mutation of hamster aminoacyl-tRNA synthetase causes apoptosis by deprivation of cognate amino acid residue. Genes Cells. 1996;1(12):1087–1099. [PubMed: 9077457]

37. Song Y, Shi Y, Carland TM, et al. p53-Dependent DNA damage response sensitive to editing-defective tRNA synthetase in zebrafish. Proc Natl Acad Sci U S A. 2016;113(30):8460–8465. [PubMed: 27402763]

38. Ladiwala U, Li H, Antel JP, Nalbantoglu J. p53 induction by tumor necrosis factor-alpha and involvement of p53 in cell death of human oligodendrocytes. J Neurochem. 1999;73(2):605–611. [PubMed: 10428056]

39. Li J, Ghiani CA, Kim JY, et al. Inhibition of p53 transcriptional activity: a potential target for future development of therapeutic strategies for primary demyelination. J Neurosci. 2008;28(24):6118–6127. [PubMed: 18550754]

40. Ma L, Yu HJ, Gan SW, et al. p53-Mediated oligodendrocyte apoptosis initiates demyelination after compressed spinal cord injury by enhancing ER-mitochondria interaction and E2F1 expression. Neurosci Lett. 2017;644:55–61. [PubMed: 28237798]

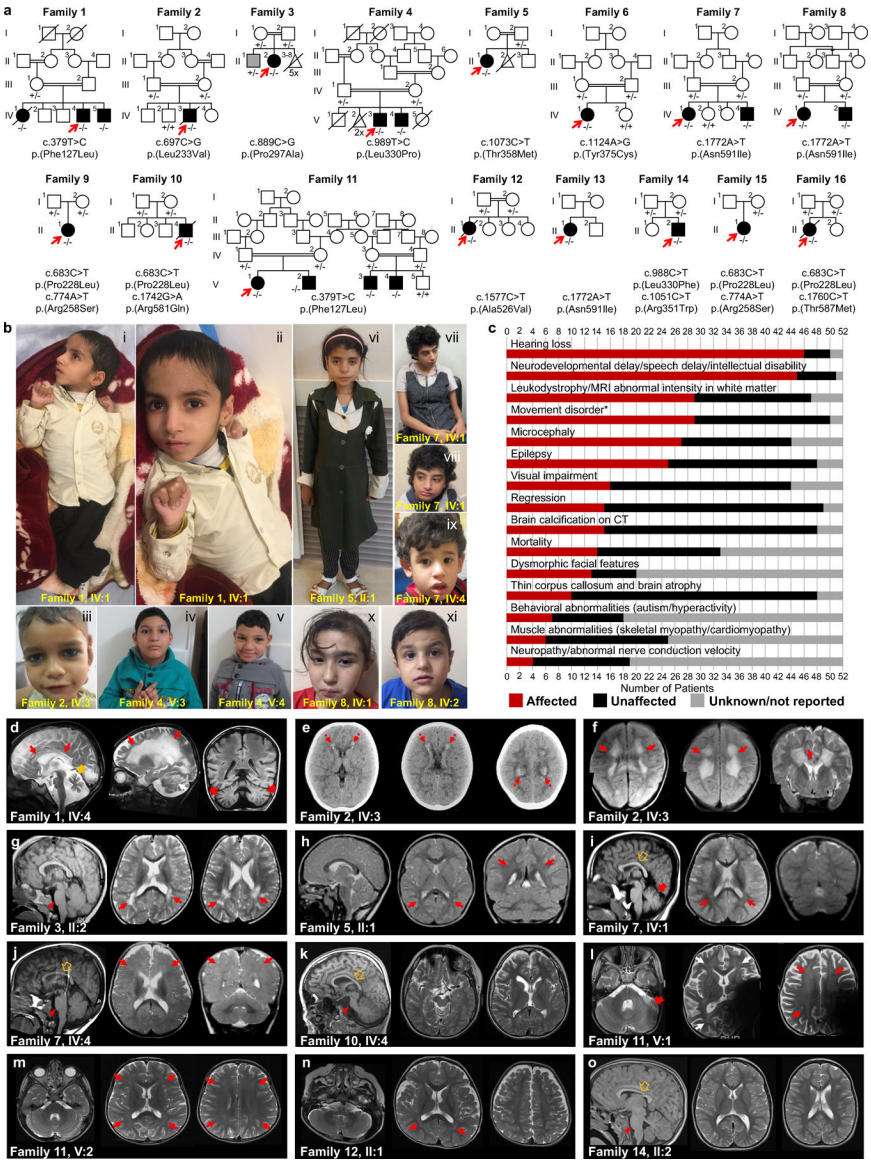

Fig. 1: Identification of Pathogenic Variants in *KARS1* in 16 families and Clinical Summary.

(**a**) Pedigrees and segregation data for the 16 families included in this study. Affected and unaffected individuals are indicated by filled and open squares(males)/circles(females), respectively. Probands are marked with red arrows. Double lines, consanguinity. Genetic diagnoses were made in 22 individuals. (**b**) Clinical characteristics of patients with homozygous *KARS1* variants, including affected individuals from family 1 (IV:4) (i, ii), family 2 (IV:3) (iii), family 4 (V:3) (iv) and (V:4) (v), family 5 (II:1) (vi), family 7 (IV:1) (vii, viii) and IV:4 (ix), and family 8 (IV:1) (x) (IV:2) (xi). Frequent clinical features include: spasticity and contractures in the limbs with clenched hands (i, ii), high forehead (iv, v, vi, vii, x), prominent nose (i, ii, iv, v, vi, vii, viii), low-set ears (i, ii, iv, v, vii, viii, ix) and short philtrum (i, ii, iv, v, vi, vii, ix, x). (**c**) Phenotype summary of features associated with *KARS1* pathogenic variants. Asterisk denotes movement disorders that include ataxia, spasticity, quadriplegia, dystonia, or chorea/tremor. (**d-o**) Neuroimaging features associated

with *KARS1* variants, with variable patterns of white matter (WM) involvement (red arrows), calcifications (red dotted arrows), pontine hypoplasia (red arrowheads), cerebellar atrophy (red thick arrows), enlargement of the cerebral CSF spaces, and corpus callosum hypoplasia (brown empty arrows).

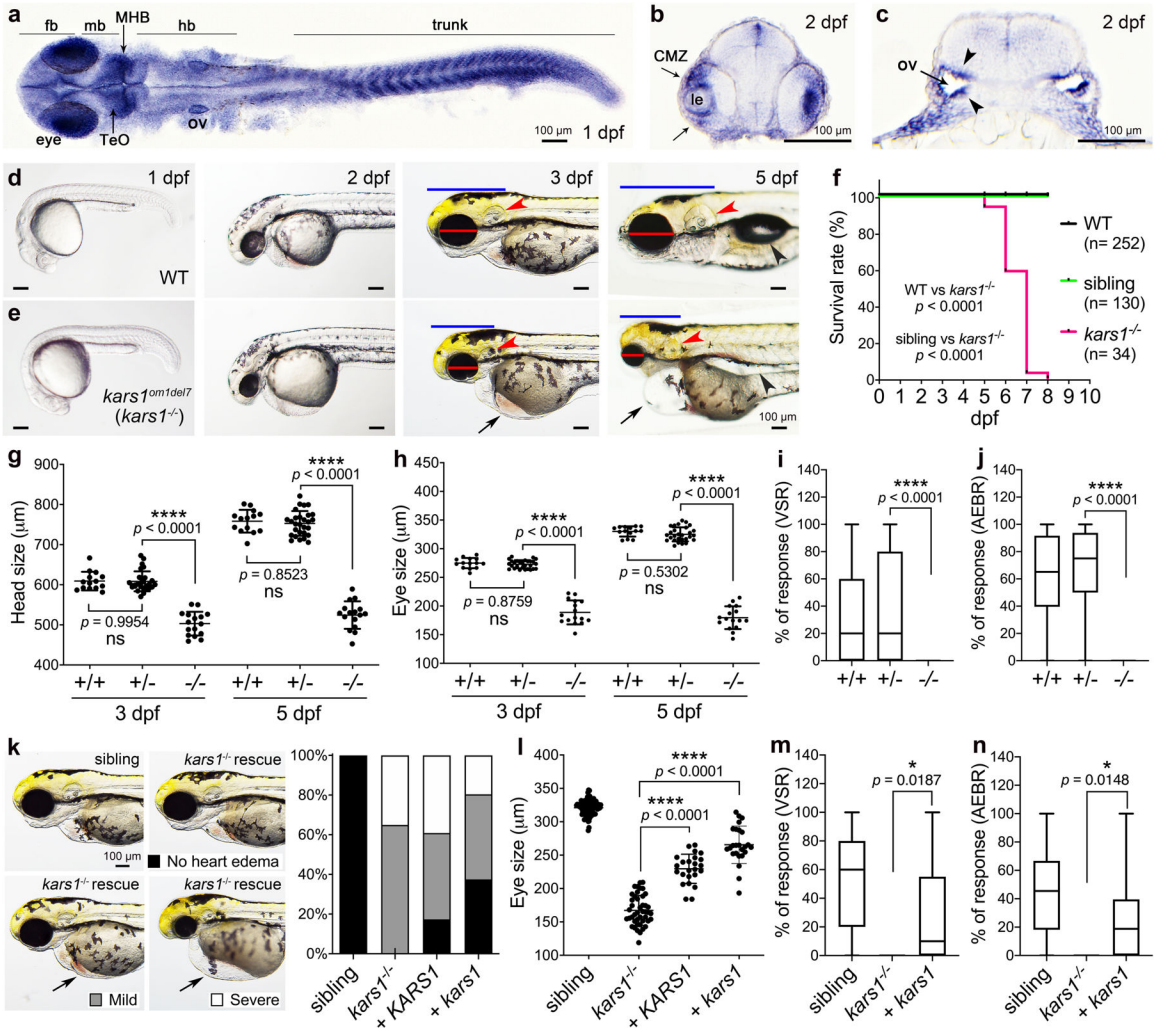

Fig. 2: The Expression of *kars1* mRNA in Embryos and *kars1* Knockouts show Gross Morphological and Behavioral Defects.

(**a**) *kars1* expression in 1 dpf (days post-fertilization) embryo. Dorsal view. (**b, c**) The cross-section of 2 dpf embryo. forebrain (fb), midbrain (mb), midbrain and hindbrain boundary (MHB), hindbrain (hb), optic tectum (TeO), otic vesicle (ov), lens (le), ciliary marginal zone (CMZ). Black arrowheads indicating the otic vesicle epithelium of otic vesicles. (**d, e**) Representative images of WT and *kars1*^{om1del7} (*kars1*$^{-/-}$) from 1 dpf to 5 dpf. Lateral view, anterior to the left. Red lines: eye diameter. Blue lines: brain size. Red arrowheads: inner ear. Black arrows: heart edema. Black arrowhead: swim bladder. (**f**) Kaplan-Meier survival curves. Time is shown in days. The Log Rank test was used for statistical analysis. (**g**, **h**) Quantification of eye and head size from *kars1*$^{+/-}$ mutant in-cross at 3 and 5 dpf. (**i**, **j**) The VSR and AEBR analyses of animals at 6 dpf from *kars1*$^{+/-}$ mutant in-cross. (**k**) Representative images of *kars1*$^{-/-}$ mutant rescue experiments and the quantification of heart edema phenotype. Animals were collected by defined heart edema categories at 3 dpf as shown in pictures and calculated in percentage of total animals. (**l**) Eye size quantification of mRNA rescue experiments at 5 dpf. (**m**, **n**) The VSR and AEBR analyses after RNA rescue at 6 dpf. n = number of animals. In (**g**, **h** and **l**), each dot represents one animal and error

bars are presented as mean ± SD. One-way ANOVA with Tukey's multiple comparisons test: ****$p < 0.0001$. In (**i**, **j**, **m** and **n**), data are plotted by box and whiskers plot and error bars indicate values from minimum to the maximum. Two-tailed unpaired *t*-test with Welch's correction: ns, not significant $p \geq 0.05$, *$p < 0.05$ and ****$p < 0.0001$.

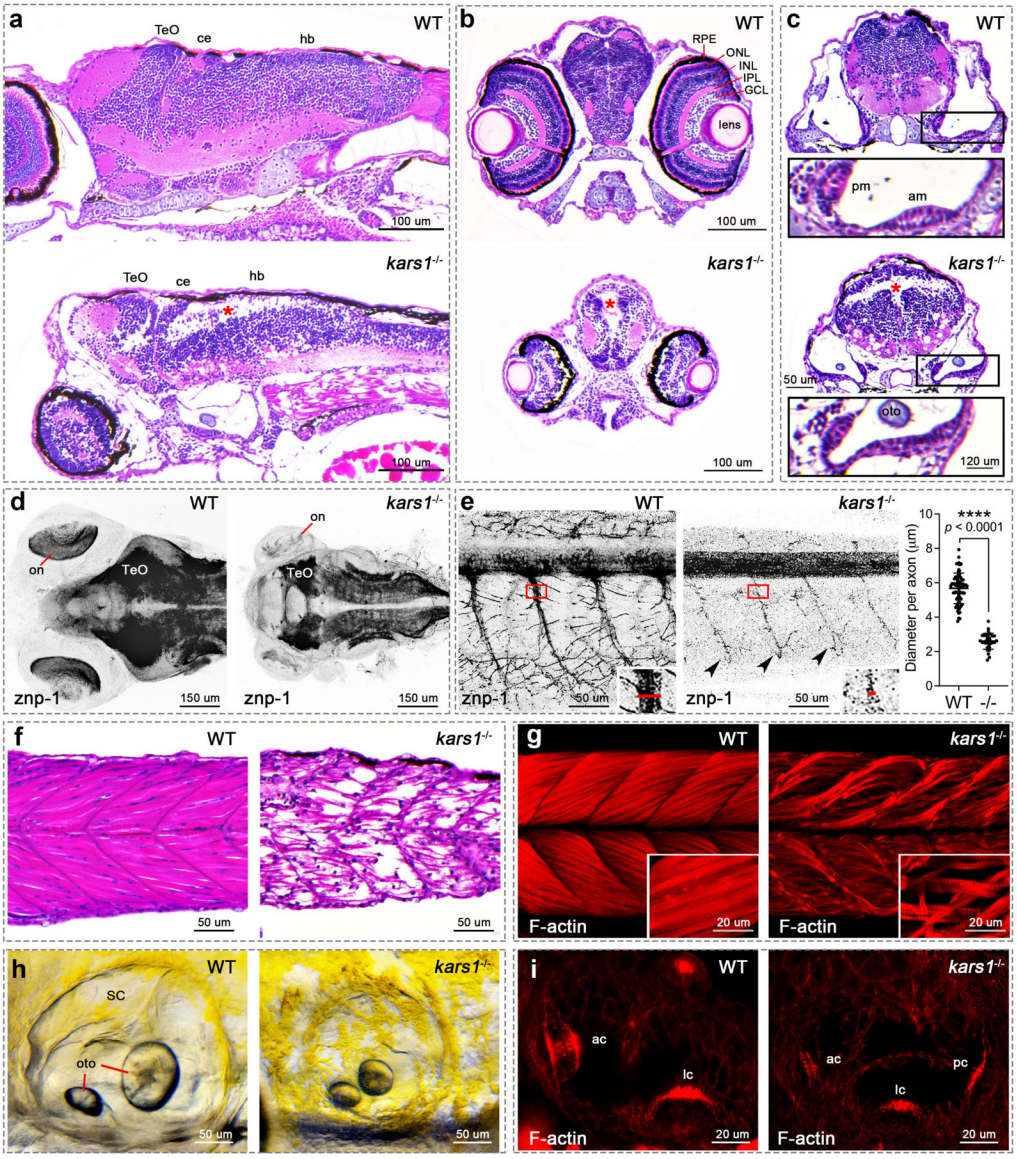

Fig. 3: The *kars1*$^{-/-}$ Larvae Display Neurological, Muscle and Inner Ear Defects by Histological Analysis at 5 dpf.

(**a**) Head region of WT and *kars1*$^{-/-}$ mutant by sagittal section. Red asterisks indicate massive loss of cell density, as well as in (**b**) and (**c**). Anterior to the left and dorsal to the top. (**b**) Eye region of WT and *kars1*$^{-/-}$ mutant by cross section. Dorsal to the top. (**c**) Inner ear region of WT and *kars1*$^{-/-}$ mutant by cross section. Dorsal to the top. Lower panels were enlarged picture from black box. (**d**) Head region of WT and *kars1*$^{-/-}$ larvae immunostained with anti-znp-1 antibody. The black-and-white fluorescent signals were inverted to negative film for a clear presentation. Dorsal view, anterior to the left. on, optic nerve. (**e**) Trunk region of WT and *kars1*$^{-/-}$ larvae which were immunostained with anti-znp-1 antibody. ImageJ was used to measure the diameter of primary motor axons as indicated by red line in the right-down panels (enlarged from red box). And the statistics shown on right hand side. Black dot indicates the diameter of each motor axon. Error bars = mean ± SD. Two-tailed unpaired nonparametric Mann-Whitney test: ****$p < 0.0001$. Black arrowheads

indicate the reduced terminal axonal branching compared to WT. Anterior to the left and dorsal to the top. (**f**) The trunk region of WT and *kars1*$^{-/-}$ larvae revealed by sagittal section. Anterior to the left and dorsal to the top. (**g**) The trunk region of WT and *kars1*$^{-/-}$ larvae revealed by confocal projections of phalloidin stained muscle fiber. Anterior to the left and dorsal to the top. The right-down panels are the higher-magnification view. (**h**) Representative bright-field images of WT and *kars1*$^{-/-}$ inner ear. Anterior to the left and dorsal to the top. Semicircular canal (SC), otolith (oto). (**i**) The red fluorescent conjugated phalloidin staining was performed to visualize the bundles (stereocilia) of hair cells in inner ear. Anterior to the left and dorsal to the top. Optic tectum(TeO), cerebellum (ce), hindbrain (hb), retinal pigment epithelium (RPE), outer nuclear layer (ONL), inner nuclear layer(INL), inner plexiform layer (IPL). ganglion cell layer (GCL), posterior macula (pm), anterior macula (am), anterior crista (ac), lateral crista (lc), posterior crista (pc).

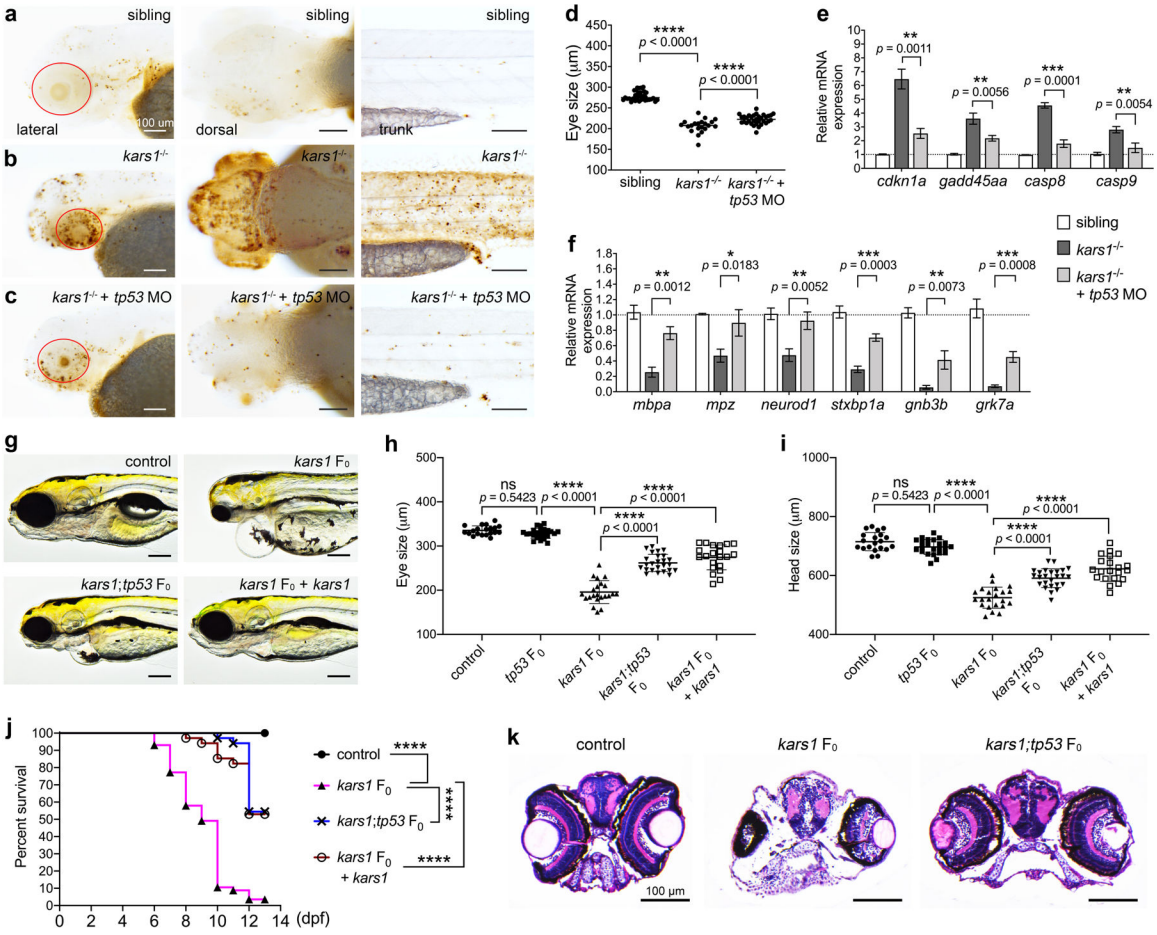

Fig. 4: Cell Apoptosis was Activated by *kars1* Loss-of-function through p53 Pathway.

(**a-c**) Representative images of sibling, *kars1*$^{-/-}$ and *kars1*$^{-/-}$ + *p53* MO at 3 dpf after TUNEL staining. Red circle indicates eye region. Scale bars = 100 μm. (**d**) The eye size measurements of sibling, *kars1*$^{-/-}$ and *kars1*$^{-/-}$ + *p53* MO at 3 dpf. (**e**) The expression levels of p53 pathway genes were examined by RT-qPCR after *p53* MO injection. (**f**) Those down-regulated genes in RNA-seq data were examined by RT-qPCR after *p53* MO injection. For (**e, f**), the expression levels were normalized to *18S* housekeeping gene. Error bars = mean ± SD. Two-tailed unpaired Student's *t*-test with Holm-Šídák multiple comparisons correction: ns, not significant $p \geq 0.05$, *$p < 0.05$, **$p < 0.01$ and ***$p < 0.001$. (**g**) Representative images of uninjected control, *kars1* F_0 mutant, *kars1;tp53* F_0 mutant, and *kars1* F_0 mutant co-injected with *kars1* mRNA at 5 dpf. Lateral view, anterior to the left. (**h**, **i**) Measurement of eye and head size in control, *tp53* F_0 mutant, *kars1* F_0 mutant, *kars1;tp53* F_0 mutant, and *kars1* F_0 mutant co-injected with 150 picogram (pg) and 200 pg of *kars1* mRNA at 5 dpf. For (**d**, **h** and **i**), each symbol represents one animal. Error bars = mean ± SD. One-Way ANOVA with Tukey's multiple comparisons test: ns, not significant $p \geq 0.05$ and ****$p < 0.0001$. (**j**) Kaplan-Meier survival curves. Time is shown in days. Log Rank test: ****$p < 0.0001$. (**k**) Histology analysis of uninjected control, *kars1* F_0 mutant and *kars1*;*tp53* F_0 mutant by cross section.

Table 1.

Summary of molecular and key clinical findings

	F1 IV:1/ F11 V:1/V:2/ V:3/V:4	F2 IV:3	F3 II:2	F4 V:3/V:4	F5 II:1	F6 IV:1	F7 IV:1/ IV:4/F8 IV:1 / IV:2/F13 II:2	F9 II:1/ F1 II:4/ F15 II
Molecular genetics summary								
Chr16 g. position	g.75674175A>G	g.75669866G>C	g.75668181C>G	g.75668081A>G	g.75665680G>A	g.75665629T>C	g.75662474T>A	g.75669880G
KARS1 c. position	c.379T>C	c.697C>G	c.889C>G	c.989T>C	c.1073C>T	c.1124A>G	c.1772A>T	c.683C>T
KARS1 p. position	F127L	L233V	P297A	L330P	T358M	Y375C	N591I	P228L
phyloP	8.92	5.66	9.87	9.34	9.84	8.02	7.95	9.59
CADD	29.7	22.2	27.0	31	29.4	32	28.1	25.5
MT	DC	DC	DC	DC	DC	DC	DC	DC
PP2	PrD	B	PrD	PrD	PrD	PrD	PrD	PrD
SIFT	D	D	D	D	D	D	D	T
gnomAD MAF	0	3.98e-6	0	0	4.95e-5	3.98e-6	7.97e-6	1.415e-4
In house MAF *	1/171678	0/171678	1/171678	1/171678	18/257204	3/212968	1/229162	39/26273(
Clinical summary								
DD	+/+/+/+/+	+	−	+/+	−	+	+/+/+/+/−	+/+/+
ID	+/+/+/+/+	+	−	+/+	−	−	+/+/+/+/−	−/−/NA
Hearing loss	+/+/+/+/+	+	+	+/+	−	+	+/+/+/+/+	+/NA/+
Regression	+/+/−/−/−	+	−	−/−	−	−	−/−/−/−/−	−/+/+
Seizures	+/−/+/−/−	+	−	+/−	−	−	−/−/+/+/+	+/+/+
Ataxia	+/−/−/−/−	−	+	−/−	−	+	+/−/−/−/−	+/−/+
Hypotonia	−/−/−/−/−	−	−	+/+	−	+	+/+/−/+/−	−/−/+
Spasticity	+/+/−/+/+	+	−	−/−	−	−	−/−/−/−/−	+/+/−
Visual impairment	−/+/+/+/−	−	NA	−/−	−	−	−/−/−/−/−	+/+/−
Absent speech	−/+/NA/+/+	−	−	−/+	+	+	+/+/−/−/−	+/+/−
Mortality	−/−/−/−/−	+	−	−/−	−	−	−/−/−/−/−	−/+/−
Dysmorphic facial features	+/+/+/+/+	+	−	+/+	+	−	+/+/+/+/−	−/−/NA
Behavioral abnormalities	−/+/−/−/−	−	−	−/+	−	−	+/+/+/+/−	−/−/NA
Leukodystrophy	+/+/+/+/−	+	+	−/+	−	NA	+/+/−/−/−	+/+/−

Genomic coordinates are listed according to GRCh37 genome build., Transcript: NM_001130089.1, MAF = minor allele frequency, phyloP scale [−14.1;6.4]

* no homozygous individuals were identified; Abbreviations: B, benign; D, Deleterious; DC, Disease causing; DD, developmental delay; F, family; ID, intellectual disability; MT, MutationTaster; NA, not assessed; PP2, PolyPhen-2; PrD, Probably damaging; T, Tolerated. The in house database consists of aggregated multiethnic cohorts from study groups.